Revealing the hidden atom in graphite by low-temperature atomic force microscopy

Stefan Hembacher*, Franz J. Giessibl*†, Jochen Mannhart*, and Calvin F. Quate‡

*Institute of Physics, Electronic Correlations and Magnetism, Experimentalphysik VI, Universität Augsburg, Universitätsstrasse 1, D-86135 Augsburg, Germany; and ‡Ginzton Laboratory, Stanford University, Stanford, CA 94305

Edited by Jan D. Achenbach, Northwestern University, Evanston, IL, and approved August 19, 2003 (received for review July 4, 2003)

Carbon, the backbone material of life on Earth, comes in three modifications: diamond, graphite, and fullerenes. Diamond develops tetrahedral sp^3 bonds, forming a cubic crystal structure, whereas graphite and fullerenes are characterized by planar sp^2 bonds. Polycrystalline graphite is the basis for many products of everyday life: pencils, lubricants, batteries, arc lamps, and brushes for electric motors. In crystalline form, highly oriented pyrolytic graphite is used as a diffracting element in monochromators for x-ray and neutron scattering and as a calibration standard for scanning tunneling microscopy (STM). The graphite surface is easily prepared as a clean atomically flat surface by cleavage. This feature is attractive and is used in many laboratories as the surface of choice for ''seeing atoms.'' Despite the proverbial ease of imaging graphite by STM with atomic resolution, every second atom in the hexagonal surface unit cell remains hidden, and STM images show only a single atom in the unit cell. Here we present measurements with a low-temperature atomic force microscope with pico-Newton force sensitivity that reveal the hidden surface atom.

The question of the existence of atoms is of central importance to the natural sciences, and the American Nobel physics laureate Richard P. Feynman has stated that in all scientific knowledge, the atomic hypothesis that "all things are made of atoms, little particles that move around in perpetual motion, attracting each other when they are a little distance apart, but repelling upon being squeezed into one another" contains the most information in the fewest words (1). Nevertheless, only 100 years ago some of the most distinguished scientists of that time were engaged in heated debates about the existence of atoms (2). To "see" atoms is therefore an important endeavor. E. W. Müller (3) achieved an important breakthrough 50 years ago with the invention of the field ion microscope that could later image single atoms on sharp tips with atomic resolution (4). Observing single atoms in real space on flat surfaces became possible 20 years ago with the invention of a marvelous instrument: the scanning tunneling microscope (STM) (5). (For a discussion of the relation between STM and other high-resolution electron microscopy techniques, see chapter 1.8 in ref. 6.) In particular, low-temperature STM provides exciting possibilities for arranging and studying matter on the nanoscale (7). STM creates images of the charge density of electrons at the Fermi level (8). In some cases, all surface atoms develop a local maximum of the charge density at the Fermi level and thus all surface atoms are observable by STM. In other cases, like GaAs (110), one type of surface atoms (As) is observable at negative sample bias and the other type (Ga) at positive sample bias (9). The graphite (0001) surface also has two types of atoms in the basis of the hexagonal surface unit cell (α and β, see Fig. 1*A*), but only one of these atom types is observed by STM, independent of the bias polarity. Theoretical investigations have shown that only the β atoms can be imaged by STM (10–14) and the α atoms remain hidden to STM. In principle, all surface atoms can be imaged with atomic force microscopy (AFM) (15). AFM probes the forces between the tip and sample, and because of the Pauli exclusion principle, the forces acting between tip and sample atoms eventually become repulsive as the tip-sample distance is reduced. However, the first static-mode AFM images of graphite using large repulsive forces obtained quasi-atomic resolution images that also showed only one protrusion per unit cell (16). Recent progress in dynamic AFM allows researchers to routinely achieve true atomic resolution on conductors and insulators (17, 18), but once again only one maximum within a hexagonal unit cell of the graphite surface was obtained in the attractive noncontact mode (19). These experimental data are in agreement with Chen's finding that tunneling current and the attractive force between a tip and a sample are proportional as shown in chapter 7 of ref. 6. However, the second atom in the unit cell should be observable with an AFM capable of detecting repulsive forces between single atoms.

Methods

In past years, our group has introduced an AFM technique with an enhanced sensitivity to short-range forces. With that method, subatomic resolution of atoms, i.e., the imaging of structures within single atoms linked to the atomic orbitals, has been demonstrated (20). Here, we also make use of the method's capability to measure tunneling current and force at the same time. Mizes *et al.* (11) show that STM images that appear to show both α and β atoms are artifacts caused by double tip effects. Because our approach allows us to measure tunneling current and force simultaneously, tip artifacts as described by Mizes *et al.* (11) can be ruled out if the STM channel only shows the β atoms. These capabilities along with a strong increase of the force sensitivity by low-temperature operation made it worthwhile to revisit the classic problem of the missing atom in the graphite surface. In our study, we use a combined low-temperature STM/AFM to simultaneously probe the charge density at the Fermi level and the total charge density of graphite by recording tunneling currents and forces, respectively. The combined STM/AFM operates in an ultrahigh vacuum. To protect it from external vibrations, it is built on a special foundation with a mass of 30 t. It is immersed in a liquid He bath cryostat, yielding a sample temperature of 4.89 K. A compact and rigid microscope design, along with excellent temperature stability, results in a very low positional drift rate of $\approx$20 pm per h. The force sensor is based on a quartz cantilever (21) with a stiffness of $k = 1{,}800$ N/m, eigenfrequency $f_0 = 18{,}076.5$ Hz, and a quality factor of $Q = 20{,}000$. The tip is prepared from a polycrystalline tungsten wire by dc etching at a voltage of 3 V. Combined STM/AFM experiments are possible by using the frequency modulation force microscopy method (22) where the cantilever is oscillating with a fixed amplitude A ($A = 300$ pm in the data displayed here). The forces acting between the oscillating tip and the sample cause a frequency shift Δf, which is related to the forces acting

This paper was submitted directly (Track II) to the PNAS office.

Abbreviations: STM, scanning tunneling microscope; AFM, atomic force microscopy.

See commentary on page 12531.

†To whom correspondence should be addressed. E-mail: franz.giessibl@physik.uni-augsburg.de.

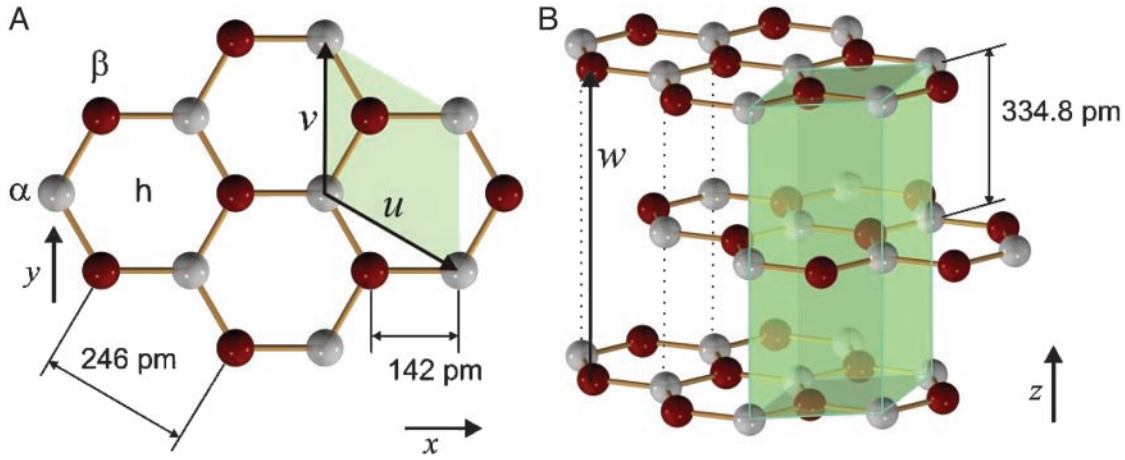

Fig. 1. Crystal structure of graphite. The unit cell is shaded in green. (*A*) Top view on the surface layer. The hexagonal surface lattice is defined by two unit vectors, *u* and *v*, in the *xy* plane with a length of 246 pm and an angle of 120° forming a honeycomb web of hexagonal rings. The basis of the lattice consists of two carbon atoms α (white) and β (red) with a distance of 142 pm. (*B*) Perspective view, showing the layered structure. The distance between layers is 2.36 times the next-neighbor distance of atoms within one layer, and the bond between layers is weak. The α atoms (white) are directly above an α atom in the layer directly underneath at a distance of 334.8 pm; the β atoms (red) are over a hollow sites (h). The unit vector *w* is parallel to the *z*-axis with a length of 669.6 pm.

between tip and sample. Because the relative tip-sample position is extremely steady, very slow scanning speeds are possible, and a very low bandwidth B can be used for detecting forces in the pN range. The noise reduction resulting from low-detection bandwidths is significant in frequency modulation AFM. Dürig *et al.* (23) have found that the signal noise in frequency modulation force microscopy is proportional to $B^{3/2}$. At low temperatures, where positional drift is insignificant, B can easily be reduced to 1/100 compared with room temperature experiments, leading to a noise level reduction to 1/1,000. The use of extremely small oscillation amplitudes of 300 pm leads to a high sensitivity to short-range forces and a strong attenuation of the long-range background forces (see section VII.A.3 in ref. 18). The low thermal drift rates enables one to perform simultaneous high-quality measurements of tunneling current and frequency shift at constant tip-sample distance.

Results

Fig. 1 displays the structure of graphite, a layered structure with a hexagonal lattice of carbon atoms linked by strong sp^2 bonds with a next-neighbor distance of only 142 pm. The layers are stacked such that three of the six atoms within a hexagon have a direct neighbor in the layer underneath at a distance of 334.8 pm. The electronic state of the valence electrons in graphite differs from the ground state configuration in atomic carbon ($1s^2 2s^2 2p^2$): one of the 2s electrons is promoted to a 2p state and three electrons in the 2s, $2p_x$, and $2p_y$ states hybridize to sp^2 states lying in the *xy* plane. The fourth valence electron is in a $2p_z$–like state (11, 12). The $2p_z$ states have the lowest bonding energy. For a single sheet of graphite, the $2p_z$ states at the α and β positions have the same energy (12). However, for crystalline graphite the overlap of the $2p_z$ states centered at the α sites leads to a lower bonding energy, leaving the $2p_z$ states centered at the β sites as the highest occupied (and lowest unoccupied) surface states. Adjacent atoms at the α and β sites are connected by extremely strong bonds, forming very durable layers in the *x-y* plane. However, in the *z*-direction these layers are weakly coupled. The force constants parallel and perpendicular to the *x-y* plane can be estimated from Raman scattering data. Nicklow *et al.* (24) find a frequency of 48.6 THz for the optical phonons parallel to the *x-y* plane and 4.2 THz in the *z*-direction. Thus, for a pair of carbon atoms the force constant is estimated to 14 N/m in the *z*-direction and 900 N/m in the *x-y* plane. Because of the softness of the lattice in the *z*-direction, the normal forces acting between tip and sample have to be kept extremely small to avoid distortions of the graphite lattice. Imaging the full graphite surface is an important milestone for imaging other soft materials, e.g., insulating organic molecules with atomic resolution.

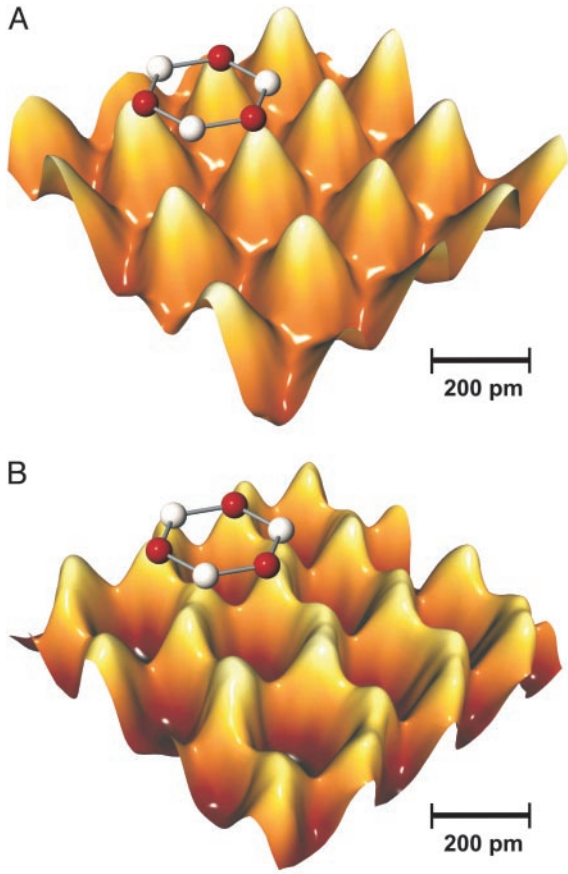

Fig. 2. (*A*) STM image of graphite. The hexagonal unit cell of graphite has two atoms in its basis, but STM shows only one of the two, forming a triagonal lattice. (*B*) AFM image of graphite (for details see Fig. 3*B*). The hexagonal carbon rings are visible, and the complete surface lattice is imaged.

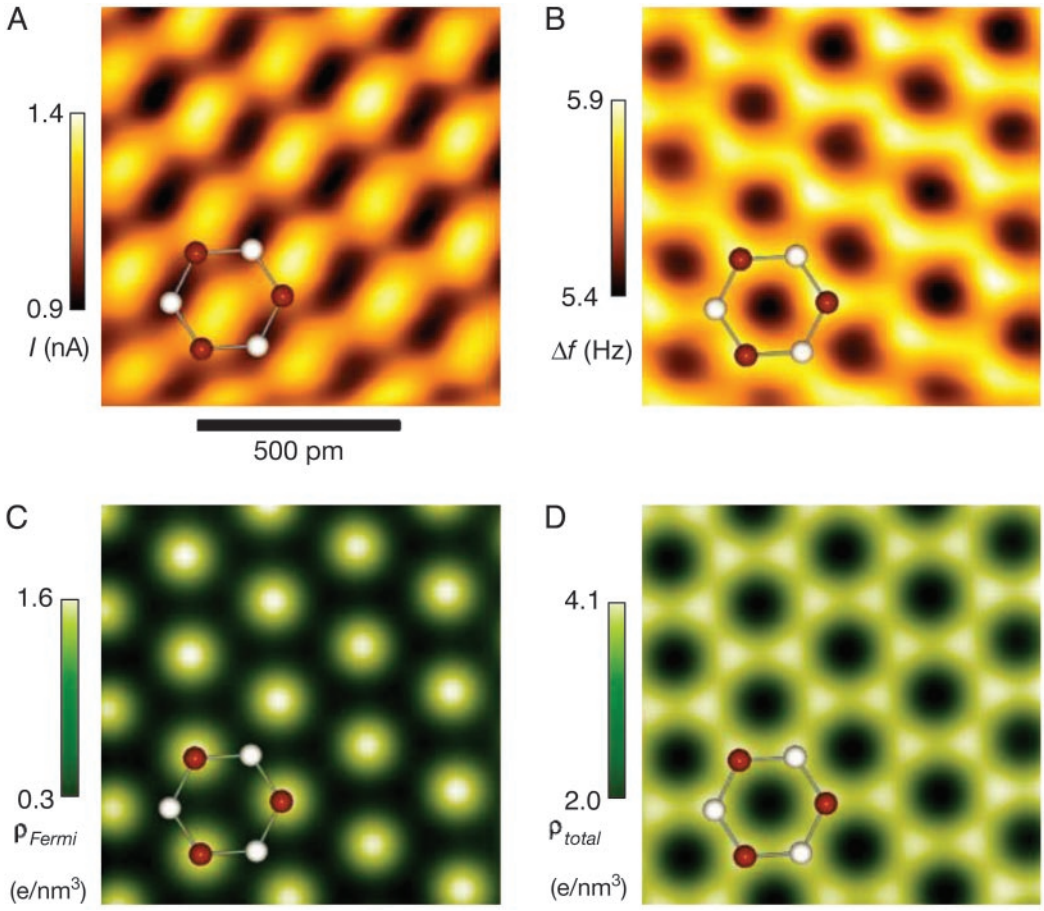

Fig. 3. Experimental and simulated STM and AFM images of graphite. One hexagonal surface unit cell with the two basis atoms α (white) and β (red) is superimposed for clarity. (*A*) Experimental image of graphite in constant-height dynamic STM mode (bias voltage +100 mV, amplitude 300 pm, scanning speed 0.2 nm/s). The tunneling current ranges from 0.9 to 1.4 nA. Only the β atoms appear in the image. The green arrow indicates a shift of the experimental STM image with respect to the AFM image by 68 pm (see text). (*B*) Experimental image of graphite in constant-height dynamic AFM mode showing both α and β atoms. The frequency shift data have been recorded simultaneously with the tunneling data shown in *A*, ranging from +5.4 to +5.9 Hz. (*C*) The calculated charge density of graphite at the Fermi level ρ_{Fermi} (after refs. 11 and 12) at a height of 200 pm over the surface plane, ranging from 0.3 to 1.6 electrons per nm^3. The maxima of ρ_{Fermi} are at the β atom positions. The STM image reflects the charge density at the Fermi level. (*D*) Calculated total charge density, also at a height of 200 pm over the surface plane, ranging from 2.0 to 4.1 electrons per nm^3. The repulsive forces that are imaged in the experimental AFM image (*B*) are increasing with the charge density; thus, a charge density plot is a good approximation for a repulsive AFM image. The experimental image in *B* and the calculated charge density shown in *D* have local maxima over α and β sites.

Fig. 2*A* shows an STM image of graphite recorded in a constant-height mode. In this STM image, only the β atoms are visible as predicted by calculations (10–14). In our experiments, we have shaped the tip by field emission and controlled collisions until relatively spherical atom images resulted and defects and steps could be imaged clearly. The sharpness of the tip also manifested itself in topographic images with a corrugation of only 20 pm; it is well established that imaging graphite with blunt tips ensues large forces, resulting in giant corrugations (25, 26). Fig. 2*B* is an AFM image of graphite, recorded with weak repulsive forces. As predicted by theory, the image shows both α atoms and β atoms. Dynamic AFM measurements provide a third experimental indication for the atomic sharpness of the tip. In the AFM image shown in Fig. 2*B*, the energy required to maintain a constant oscillation amplitude A is measured simultaneously with the frequency shift and average tunneling current. In the data presented here, the extra energy required for keeping A constant when the tip oscillates close to the sample was negligible, whereas flat tips with a large contact area to the sample cause unstable tip oscillations and require significant energy for maintaining a constant amplitude.

Fig. 3 shows experimental and theoretical images of the graphite surface in STM and AFM mode. Fig. 3*A* is a constant-height image of the tunneling current, whereas Fig. 3*B* is the frequency shift data taken simultaneously with the data of Fig. 3*A*. Both α and β atoms within a hexagonal unit cell are clearly visible in this AFM image. The positive sign in the frequency shift indicates that repulsive short-range forces between tip and sample are acting. The repulsive forces are attributed to the overlap of 5s-, 5p-, and 6s-like states of the tungsten tip with the sample states, as observed with transition metal tips imaging silicon samples (27). Because the energy of these states is significantly below the Fermi energy, they do not contribute to the tunneling current. However, the electrons in the strongly bonded 5s-, 5p-, and 6s–like states have a larger average distance from the W nucleus than the electrons in the mobile 5d–like tunneling states. The forces that act between tip and sample can be estimated from the experimental parameters. With the oscillation amplitude of 300 pm, the cantilever spring constant of 1,800 N/m and the eigenfrequency of 18,076.5 Hz, the normalized frequency shift (17, 28) $\gamma = kA^{3/2}\Delta f/f_0$ is + 2.7 fNm$^{0.5}$. The variation of γ with distance was experimentally determined to $d\gamma/dz = -2.8$ aNm$^{0.5}$/pm, yielding an estimate for the total interaction force of 248 pN over α sites, 250 pN over β sites, and

223 pN over hollow sites (estimated by using equation 12 in ref. 28). It is interesting to note that the force over β sites is slightly larger than over α sites. A simple analysis would lead one to expect the opposite, because the α sites have a direct neighbor underneath and thus should be harder. However, Whangbo *et al.* (29) found that for large tip atoms such as tungsten, the β sites appear to be harder. Fig. 3*C* shows an approximation for the charge density at the Fermi level ρ_{Fermi} at a height of 200 pm over the surface layer. Fig. 3*C* depicts the charge density according to 1-fold occupied p_z states centered at the β sites. Because the tunneling current is proportional to ρ_{Fermi}, Fig. 3*C* is a calculated image of Fig. 3*A*. The corresponding states are p_z states centered at the β positions. The STM image reflects a convolution of the tip state with the sample state. For tungsten tips, calculations show that $5d_{z^2}$-like states carry the tunneling current (30). The elongation of the experimental atom images in the STM channel and the displacement relative to the AFM channel of 68 pm along the diagonal of the *x-y* plane indicate a tilt of the $5d_{z^2}$-like tip states (27). Fig. 3*D* shows an estimate of the total charge density of graphite (also at $z = 200$ pm). The total charge density is calculated by taking all C $1s^2$, $2sp^2$, and $2p_z$ states into account (see refs. 11 and 12). The two basis atoms α and β appear at a similar brightness. It is interesting to note that the β atoms are shifted by 68 pm in the experimental STM and AFM images shown in Fig. 3 *A* and *B*. This shift is small compared with the size of the tungsten tip atom (274 pm) and reflects the different physical origin of tunneling current and repulsive force.

Conclusion

In summary, we have found the hidden surface atom in the unit cell of graphite and shown the capability of AFM to gather information on surfaces that are only partially accessible by STM, emphasizing an additional facet of studying matter on the atomic scale. The successful imaging of the complete surface lattice of graphite is encouraging regarding the possibility of imaging other soft matter with atomic resolution by force microscopy.

We thank H. Bielefeldt and K. Wiedenmann for help with the construction of the microscope and M. Herz and T. Kopp for discussions. This work is supported by the Bundesministerium für Bildung und Forschung (Project 13N6918).

1. Feynman, R. P., Leighton, R. B. & Sands, M. (1963) *The Feynman Lectures on Physics I-1-2* (Addison–Wesley, Reading, MA).
2. Lindley, D. (2001) *Boltzmann's Atom: The Great Debate That Launched a Revolution in Physics* (Free Press, New York).
3. Müller, E. W. (1951) *Z. Phys.* **131,** 136–142.
4. Müller, E. W. & Bahadur, K. (1956) *Phys. Rev.* **102,** 624–631.
5. Binnig, G., Rohrer, H., Gerber, Ch. & Weibel, E. (1982) *Phys. Rev. Lett.* **49,** 57–60.
6. Chen, C. J. (1993) *Introduction to Scanning Tunneling Microscopy* (Oxford Univ. Press, New York).
7. Manoharan, H., Lutz, C. P. & Eigler, D. M. (2000) *Nature* **403,** 512–515.
8. Tersoff, J. & Hamann, D. R. (1983) *Phys. Rev. Lett.* **50,** 1998–2001.
9. Feenstra, R. M., Stroscio, J. A., Tersoff, J. & Fein, A. P. (1987) *Phys. Rev. Lett.* **58,** 1192–1195.
10. Batra, I. P., Garcia, N., Rohrer, H., Salemink, H., Stoll, E. & Ciraci, S. (1987) *Surf. Sci.* **181,** 126–138.
11. Mizes, H. A., Park, S. & Harrison, W. A. (1987) *Phys. Rev. B* **36,** 4491–4494.
12. Mizes, H. A. (1987) Ph.D. thesis (Stanford Univ., Stanford, CA).
13. Binnig, G., Fuchs, H., Gerber, Ch., Rohrer, H., Stoll, E. & Tosatti, E. (1986) *Europhys. Lett.* **1,** 31–36.
14. Tománek, D., Louie, S. G., Mamin, H. J., Abraham, D. W., Thomson, R. E., Ganz, E. & Carke, J. (1987) *Phys. Rev. B* **35,** 7790–7793.
15. Binnig, G., Quate, C. F. & Gerber, Ch. (1986) *Phys. Rev. Lett.* **50,** 930–933.
16. Albrecht, T. R. & Quate, C. F. (1988) *J. Vac. Sci. Technol. A* **6,** 271–274.
17. Morita, S., Wiesendanger, R. & Meyer, E., eds. (2002) *Noncontact Atomic Force Microscopy* (Springer, New York).
18. Giessibl, F. J. (2003) *Rev. Mod. Phys.* **75,** 949–983.
19. Hölscher, H., Allers, W., Schwarz, U. D., Schwarz, A. & Wiesendanger, R. (2000) *Phys. Rev. B* **62,** 6967–6970.
20. Giessibl, F. J., Hembacher, S., Bielefeldt, H. & Mannhart, J. (2000) *Science* **289,** 422–425.
21. Giessibl, F. J. (1998) *Appl. Phys. Lett.* **73,** 3956–3958.
22. Albrecht, T. R., Grütter, P., Horne, D. & Rugar, D. (1991) *J. Appl. Phys.* **69,** 668–673.
23. Dürig, U., Züger, O. & Stalder, A. (1992) *J. Appl. Phys.* **72,** 1778–1798.
24. Nicklow, R., Wakabayashi, N. & Smith, H. G. (1972) *Phys. Rev. B* **5,** 4951–4962.
25. Soler, J. M., Baro, A. M., García, N. & Rohrer, H. (1986) *Phys. Rev. Lett.* **57,** 444–447.
26. Pethica, J. B. (1986) *Phys. Rev. Lett.* **57,** 3235.
27. Herz, M., Giessibl, F. J. & Mannhart, J. (2003) *Phys. Rev. B* **68,** 45301.
28. Giessibl, F. J. & Bielefeldt, H. (2000) *Phys. Rev. B* **61,** 9961–9964.
29. Whangbo, M. H., Liang, W., Ren, J., Magonov, S. N. & Wawkuschewski, A. (1994) *J. Phys. Chem.* **98,** 7602–7607.
30. Ohnishi, S. & Tsukada, M. (1989) *Solid State Commun.* **71,** 391–394.